Digest Journal of Nanomaterials and Biostructures Vol. 12, No. 4, October-December 2017, p. 1247-1257

TWO-TEMPERATURE MODEL USING THE CATTANEO-VERNOTTE EQUATION IN THE ANISIMOV-NOLTE MODEL FOR APPLICATION IN LASER ADDITIVE MANUFACTURING

M. OANE[a], I. N. MIHĂILESCU[a*], A. BUCĂ[b], C. RISTOSCU[a],
G. POPESCU-PELIN[a], C. M. TICOȘ[a]
[a]*National Institute for Laser, Plasma and Radiation Physics, 409 Atomistilor street, 077125, Magurele, Ilfov, Romania*
[b]*University of Bucharest, Faculty of Physics, 077125, Magurele, Ilfov, Romania*

Current laser technology is based on powerful systems generating pulses of very short duration. To describe the interaction with matter of these pulses, the application of thermal models involving finite speed heat transfer and not infinite as in the standard Two-Temperature Model is required. This paper is reporting on the development of a unique Cattaneo-Vernotte equation in a model which provides information about 3D thermal fields, surface temperature, and steady state temperature quantum effects for laser irradiation of matter. The integral transform technique, merging the Anisimov and Nolte models with the Cattaneo - Vernotte equation, is used.

(Received October 26, 2017; Accepted December 20, 2017)

Keywords: Two-temperature model; finite velocity of heat transfer; Cattaneo-Vernotte equation; Anisimov-Nolte model; laser transverse modes

1. Introduction

The two-temperature model (TTM) by laser interaction with solids was proposed by the Russian School of Theoretical Physics almost 35 years ago (for a review see Ref. 1). Many developments followed since then in specialized literature (see *e.g*. Refs. 2-17). The solution to TTM can be inferred by solving two coupled differential equations. A simplified TTM was introduced by Nolte in 1997 [2]. In 2012 a TTM with an infinite speed of heat propagation [3] was proposed by the current team.

TTM developments can also stand for an essential theoretical tool to be used in connection with the new strongly emerging technologies based on laser additive manufacturing (LAM), also known as solid freeform fabrication, digital manufacturing, or e-manufacturing [18]. LAM is developing via material incremental manufacturing (MIM) and implies layer by layer shaping and consolidation of powder materials to a given configuration [18, 19]. LAM processes are typically applied for manufacturing prototypes while miniaturized features of 100-200 μm can be easily approached [18, 20].

In practice, the computer aided design (CAD) model of the object to be produced is mathematically sliced into thin layers. The object is then produced and consolidated under the action of a scanning laser beam [18]. One therefore expects a high progress of the simulation process when introducing the complex, more suitable TTM.

The present paper reports on a new development of TTM, namely by considering a finite velocity of heat transfer.

On the other hand, a quite powerful method was developed to solve the Fourier heat transfer equation [21-29]. In this contribution, it was intended to combine the Nolte model with the Cattaneo-Vernotte equation [1], in order to develop a unique heat equation for the "classical" TTM to be further extended to LAM description. Starting from some plausible physical simplifications,

* Corresponding author: ion.mihailescu@inflpr.ro

one can get information about 3D thermal fields, surface temperature, and steady state quantum effects that usually take place at the laser-metal interaction interface.

2. Model

The TTM consists of the two coupled equations [3]:

$$A \cdot T_e \left(\frac{dT_e}{dt} \right) = K \left(\frac{\partial^2 T_e}{\partial x^2} + \frac{\partial^2 T_e}{\partial y^2} + \frac{\partial^2 T_e}{\partial z^2} \right) - G \left(T_e - T_i \right) + P_a(\vec{r}, t) , \tag{1a}$$

$$C_i \left(\frac{dT_i}{dt} \right) = G \left(T_e - T_i \right) . \tag{1b}$$

Here, T_e and T_i are the electron and phonon/lattice temperatures, respectively. G is the coupling factor between electrons and phonons. $P_a(\vec{r}, t)$ is the heat source, which is given by the laser-matter interaction. The interaction can be of the steady state classical or the quantum mechanical type. A is the electron heat capacity and K is the thermal conductivity of the sample. C_i is the volume specific heat capacity of the lattice.

G can be determined from the equation [7]:

$$G = \frac{\pi^2 m N v^2}{6 \tau T_i} \cdot \left(\frac{T_e}{T_i} \right)^4 \times \int_0^{T_e / T_d} \left[x^4 / \left(e^x - 1 \right) \right] \cdot dx \tag{2}$$

where m is the electron mass, N is the conductive electrons density, v is the velocity of sound in the solid, τ is the electron-phonon collision time and T_D is the Debye temperature.

In Ref. 3 we have shown that $A \approx 100$ J/(m^{3}K^2) and $C_i \approx 3 \times 10^6$ J/m^{3}K. These data refer to metals such as Cu, Au and Ag. Because $C_i >> A \cdot T_e$, a first approximation may be written as follows:

$$K \left(\frac{\partial^2 T_e}{\partial x^2} + \frac{\partial^2 T_e}{\partial y^2} + \frac{\partial^2 T_e}{\partial z^2} \right) - C_i \frac{\partial T_i}{\partial t} = - P_a(\vec{r}, t) . \tag{3}$$

Next, the following formula from the Nolte model [2] can be used:

$$T_i = \kappa T_e \tag{4}$$

where

$$\kappa = \frac{\tau_L}{\tau_L + \tau_i} \tag{5}$$

(τ_i – is the lattice cooling time and τ_L - is the laser pulse time).
In consequence, the result is:

$$\frac{\partial T_i}{\partial t} = \kappa \frac{\partial T_e}{\partial t} \tag{6}$$

Thus, a generalized equation can be inferred, using the Cattaneo-Vernotte version of the heat equation (3) as follows:

$$K\left(\frac{\partial^2 T_e}{\partial x^2}+\frac{\partial^2 T_e}{\partial y^2}+\frac{\partial^2 T_e}{\partial z^2}\right)-C_i\kappa\frac{\partial T_e}{\partial t}-\frac{K\tau_0}{\gamma}\frac{\partial^2 T_e}{\partial t^2}=-P_a(\vec{r},t) \tag{7}$$

Thus, the following is obtained:

$$\left(\frac{\partial^2 T_e}{\partial x^2}+\frac{\partial^2 T_e}{\partial y^2}+\frac{\partial^2 T_e}{\partial z^2}\right)-\frac{1}{\gamma}\frac{\partial T_e}{\partial t}-\frac{\tau_0}{\gamma}\frac{\partial^2 T_e}{\partial t^2}=-\frac{P_a(\vec{r},t)}{K} \tag{8}$$

with:

$$\gamma = \frac{K}{C_i\kappa} \text{ (thermal diffusivity).} \tag{9}$$

Under a generalized form, one can express P_a as:

$$P_a = \sum_{m,n} I_{mn}(y,z)\left(\alpha_{mn}e^{-\alpha_{mn}x}\right)\left(1-r_{Smn}\right)+r_{Smn}\delta(x)+q.c.)\cdot(1+\tau_0\cdot\delta(t))\cdot(u(t)-u(t-\tau_L)) \ . \tag{10}$$

Here, $I_{mn}(y,z)$ is the laser transverse mode {m,n} intensity, α_{mn} is the linear absorption coefficient for the mode {m,n}, r_{Smn} is the surface absorption coefficient for the transverse laser mode {m,n}, and q.c. are quantum steady state corrections. u is the step function, which is defined as: u(t)={0, if t<0 and 1, if t>0}. $\delta(x)$ is the Dirac function while τ_L is the laser pulse duration τ_0 is the relaxation time, with the physical significance that $\sqrt{\frac{\gamma}{\tau_0}}$ is the speed of thermal waves inside the target sample. For continuous irradiation, this time becomes the exposure time.

In the model in question, which uses a rectangular form of the pulse, as compared to the Nolte model [2], which uses an exponential type form for the time pulse, the equivalence of the two models by hypothesizing that the intensity *versus* time plots covers the same area is being formulated. Therefore, an equivalent time constant τ_L for the rectangular pulse can be obtained.

3. Solutions

The single equation (8) can be solved using the integral transform technique [18-26] by calculating the eigen-functions and eigen-values. The target was a parallelepiped of dimensions a, b and c.

The following differential equation from classical theory [18-26] should be considered:

$$\frac{\partial^2 K_x}{\partial x^2}+\mu_i^2 K_x = 0, \tag{11}$$

with the solution:

$$K_x = \cos(\mu_i \cdot x) + \frac{h}{K \lambda_i} \sin(\mu_i \cdot x). \quad (12)$$

Here, K_x are the eigen-functions, $\mu_i, \beta_l, \lambda_j$ the eigen-values, h is the heat transfer coefficient and K, the thermal conductivity.

The boundary conditions read:

$$\left[\frac{\partial K_x}{\partial x} - \frac{hK_x}{K}\right]_{x=0} = 0 \quad ; \quad \left[\frac{\partial K_x}{\partial x} + \frac{hK_x}{K}\right]_{x=a} = 0. \quad (13)$$

Under these boundary conditions, the following eigen-values, μ_i can be inferred:

$$2\cot(\mu_i a) = \frac{\mu_i K}{h} - \frac{h}{K \mu_i}. \quad (14)$$

In the same manner, the above formalism may be extended to y and z coordinates.

By integral transform technique the following solution [25] is obtained:

$$T_e = \sum_{i=1}^{\infty}\sum_{l=1}^{\infty}\sum_{j=1}^{\infty} f(\mu_i, \beta_l, \lambda_j) \cdot g(\mu_i, \beta_l, \lambda_j, t) \cdot K_x(\mu_i, x) \cdot K_Y(\beta_l, y) \cdot K_z(\lambda_j, z) \cdot \quad (15)$$

By limitation to the first ten terms (for i, l, j) the following analytical solution is obtained:

$$T_e = \sum_{i=1}^{10}\sum_{l=1}^{10}\sum_{j=1}^{10} f(\mu_i, \beta_l, \lambda_j) \cdot g(\mu_i, \beta_l, \lambda_j, t) \cdot K_x(\mu_i, x) \cdot K_Y(\beta_l, y) \cdot K_z(\lambda_j, z) \cdot \quad (16)$$

The current simulation shows that only the estimation of T_e with ten terms is justified, as it generates an error that is less than 10^{-2} ºC [23].

Thus:

$$f(\mu_i, \beta_l, \lambda_j) = \int_0^a \int_0^b \int_0^c K_x(\mu_i, x) \cdot K_Y(\beta_l, y) \cdot K_z(\lambda_j, z) \cdot P_a(x, y, z, t) dx dy dz. \quad (17)$$

Through direct and inverse Laplace transform for the variable tone the following is obtained:

$$g(\mu_i, \beta_l, \lambda_j, t) = e^{\left(\frac{-1-\gamma\cdot\eta_{ilj}}{2\tau_0}\right)\cdot t} \cdot \frac{4\,\tau_0\,A \cdot e^{\frac{\gamma\cdot\eta_{ilj}\cdot t}{\tau_0}}}{\left(1 - e^{\frac{\gamma\cdot\eta_{ilj}\cdot t}{\tau_0}}\right)\gamma\,K\left(\eta_{ilj}^2 - \frac{1}{\gamma^2}\right)} - e^{\left(\frac{-1+\gamma\cdot\eta_{ilj}}{2\tau_0}\right)\cdot t} \cdot \frac{4\,\tau_0\,A}{\left(1 - e^{\frac{\gamma\cdot\eta_{ilj}\cdot t}{\tau_0}}\right)\gamma\,K\left(\eta_{ilj}^2 - \frac{1}{\gamma^2}\right)} -$$

$$-\left(4\cdot\frac{\tau_0\cdot A}{\gamma\cdot K}\left(\eta_{ilj}-\mu_i^2\cdot e^{\left(\frac{-1-\gamma\cdot\eta_{ilj}}{2\tau_0}\right)\cdot t}\cdot\tau_0\cdot u(t)-\beta_l^2\cdot e^{\left(\frac{-1-\gamma\cdot\eta_{ilj}}{2\tau_0}\right)\cdot t}\cdot\tau_0\cdot u(t)-\lambda_j^2\cdot e^{\left(\frac{-1-\gamma\cdot\eta_{ilj}}{2\tau_0}\right)\cdot t}\cdot\right.\right.$$
$$\left.\left.\tau_0 u(t)+\mu_i^2\cdot e^{\left(\frac{-1+\gamma\cdot\eta_{ilj}}{2\tau_0}\right)\cdot t}\cdot\tau_0\cdot u(t)+\beta_l^2\cdot e^{\left(\frac{-1+\gamma\cdot\eta_{ilj}}{2\tau_0}\right)\cdot t}\cdot\tau_0\cdot u(t)+\lambda_j^2\cdot e^{\left(\frac{-1+\gamma\cdot\eta_{ilj}}{2\tau_0}\right)\cdot t}\cdot\tau_0\cdot\right.\right.$$
$$\left.\left.u(t)\right)\right)\cdot\eta_{ilj}^{-1}\cdot\left(\left(-\frac{1}{\gamma}+\eta_{ilj}\right)\left(\frac{1}{\gamma}+\eta_{ilj}\right)\right)^{-1}. \qquad (18)$$

Here:

$$\eta_{ilj}^2=\frac{1}{\gamma^2}-4\left(\mu_i^2+\beta_l^2+\lambda_j^2\right)\cdot\frac{\tau_0}{\gamma} \qquad (19)$$

and u(t)stands for the unit step function.

Next, based on the T_e value obtained, T_i can be calculated, using Eq. (4).

4. Analytical simulations

The new model was applied to simulate the thermal field (in arbitrary units) for the ultra-short laser pulses heating of an Au bulk sample. The Au target dimensions are (10 x 4 x 4) mm^3.

The thermal field evolution depends on the relaxation time which assumes a finite speed of the thermal waves: $v=\sqrt{\frac{\gamma}{t_0}}$. Here, γ is Au thermal diffusivity and t_0 is the relaxation time.

The spatial laser intensity distribution is assumed to be Gaussian (TEM_{00}) and Figs. 1-5 correspond to the case when x=5 mm and y=0 mm, respectively.

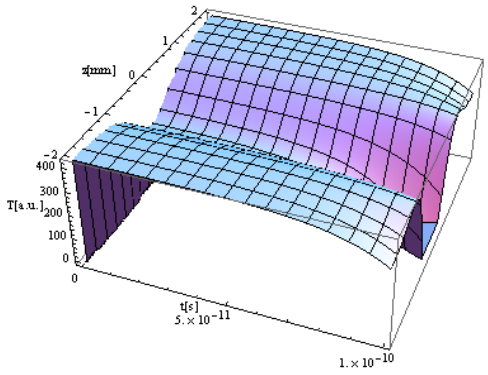

Fig. 1: Thermal field inside the Au bulk target for a single pulse irradiation with a duration of 10^{-10}s and a relaxation time of 10^{-11}s

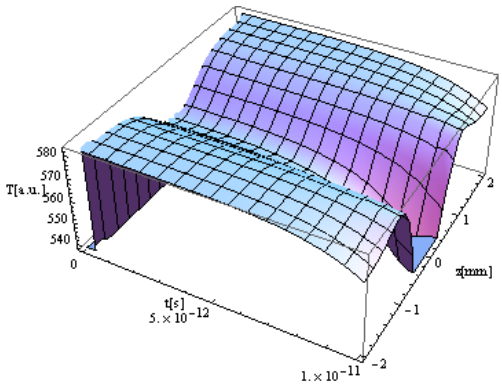

Fig. 2. Thermal field inside the Au bulk target for a single pulse irradiation with a duration of 10^{-11}s, and a relaxation time of 10^{-12}s

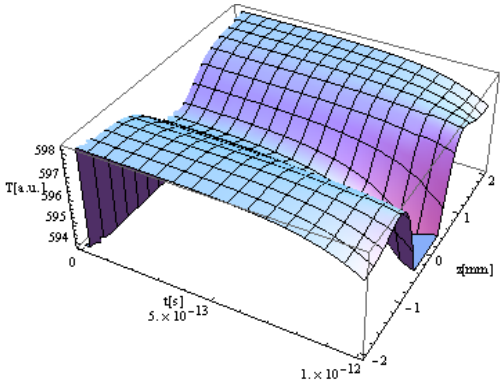

Fig. 3. Thermal field inside the Au bulk target for a single pulse irradiation with a duration of 10^{-12}s, and a relaxation time of 10^{-13}s

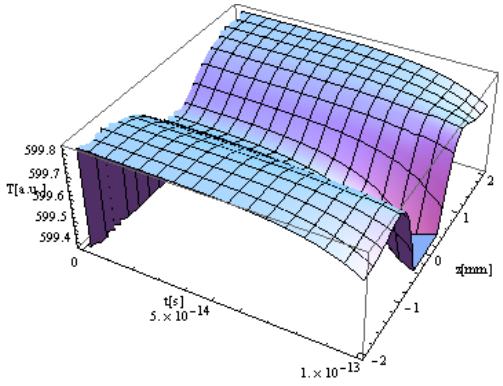

Fig. 4. Thermal field inside the Au bulk target for a single pulse irradiation with a duration of 10^{-13}s, and a relaxation time of 10^{-14}s

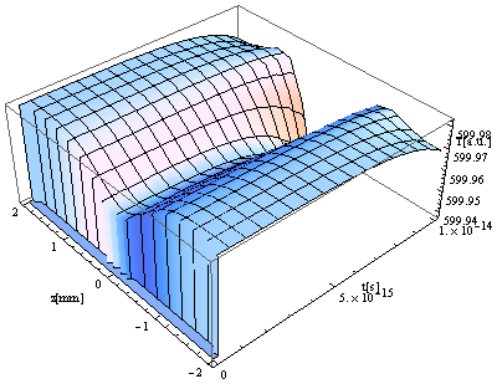

Fig. 5. Thermal field inside the Au bulk target for a single pulse irradiation with a duration of 10^{-14}s, and a relaxation time of 10^{-15}s

The general trend visible from Figs. 1-5 is that the lower the relaxation time, the higher the thermal wave speed is. Consequently, the target temperature becomes more and more uniform (the arbitrary units from Figs. 1-6 are self-consistent). If the pulse duration and relaxation time are further decreased the limit of the classical Fourier case is reached, when the thermal wave velocity is infinite and the thermal distribution is almost constant. This evolution is depicted in Fig. 6.

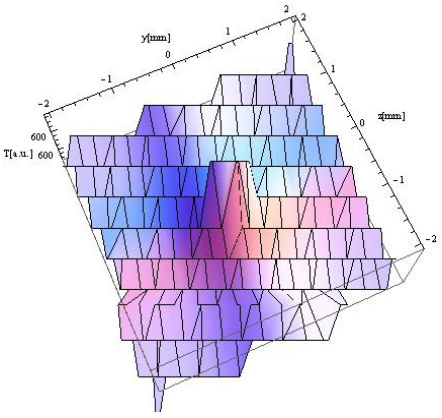

Fig. 6. Thermal field distribution inside the Au bulk target immediately after a single pulse irradiation with a duration of 10^{-14}s, and a relaxation time of 0 s (a similarity to the classical Fourier case can be seen)

Fig. 7 illustrates the temperature in the point of Cartesian coordinates (x=5 mm, y=0 mm and z=0 mm) versus the relaxation time, when x is the propagation direction.

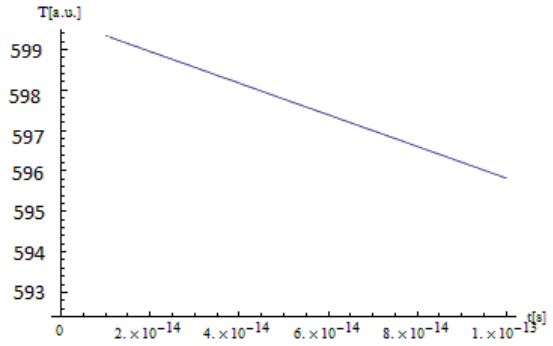

Fig. 7. Temperature in the point of x=5 mm, y=0 mm and z=0 mm; inside the Au bulk target; when the relaxation time varies from 10^{-13}s (pulse duration10^{-12}s) to 10^{-14}s (pulse duration 10^{-13}s)

In Fig. 7 a decrease of temperature with the increase of relaxation/duration time can be noticed.

Figs. 8 and 9 illustrate the temperature field for a given value of relaxation time and pulse duration.

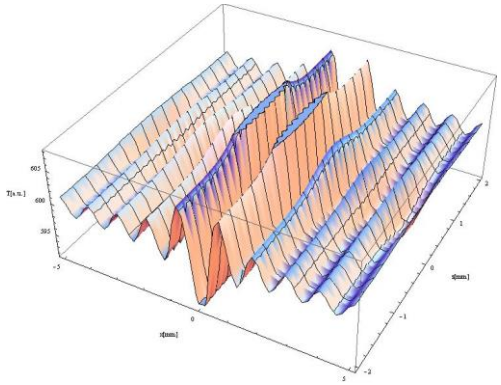

Fig. 8. Temperature field (x - the direction of laser beam propagation, y=0 mm) inside the Au bulk target for a single pulse irradiation with a duration of 10^{-13}s, and a relaxation time of 10^{-14}s

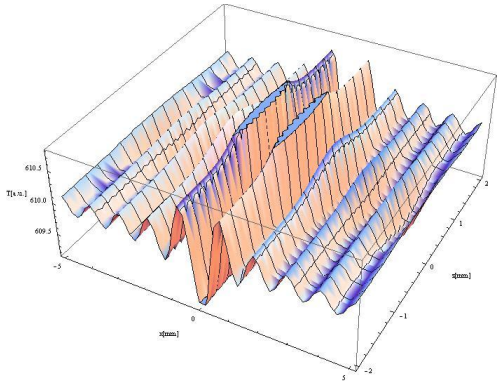

Fig. 9. Temperature field (x - the direction of laser beam propagation, y=0 mm) inside the Au bulk target for a single pulse irradiation with a duration of 10^{-14}s, and a relaxation time of 10^{-15}s

The average temperature variation in Fig. 8 is about 10 a.u. while in Fig. 9 is 1 a.u. only, *i.e.* the temperature distribution gets narrower when decreasing the relaxation time/ pulse duration. It should be mentioned that the simulations were conducted so that 1 a.u. is identical in all figures.

5. "FLAT" beams

A flat spatial distribution beam in intensity shall be considered to be compared with the TEM_{00} case. The target parameters and the total power of the incident laser beam shall be kept unchanged. Fig. 10 is illustrating the thermal field inside the Au bulk target for a single pulse irradiation of 10^{-13}s, a relaxation time of 10^{-14}s and a flat spatial distribution of the incident laser beam.

When comparing Fig. 10 and Fig. 4 (flat "case" versus TEM_{00} "case"), it can be seen that in the flat laser beam situation, the thermal distribution is almost constant in space and time.

Another key parameter is the heat transfer coefficient, which for the current simulations, except for Fig. 11, was chosen to be $h=10^{-6}$ $Wmm^{-2}K^{-1}$ [30]. In Fig. 11 $h\rightarrow 0$ [30] was considered.

When comparing Fig. 11 and Fig. 12 it can be noted that due to the fact that there is no heat exchange between the target and the surrounding medium (high vacuum conditions), figure 11 is showing larger temperature variations as opposed to the thermal field from figure 12.

Fig. 13 goes back to the situation of an incident laser beam TEM_{00}, when $h\rightarrow 0$ was considered. Fig. 13, which presents an almost uniform thermal distribution with an increasing tendency in time, may be compared with Fig. 4 and Fig. 10.

Fig. 14 and Fig.15 illustrate the thermal field inside the Au bulk target for a single pulse irradiation of 10^{-13}s, and a relaxation time of 10^{-14}s, for the TEM_{00} for the laser beam, when $h=10^{-6}$ $Wmm^{-2}K^{-1}$ (Fig. 14) and $h\rightarrow 0$ (Fig. 15). Fig. 15 is showing larger thermal fluctuations as opposed to Fig. 14. The reason is, in the opinion of the current team, similar: the very low heat transfer target loss from the situation presented in Fig. 15.

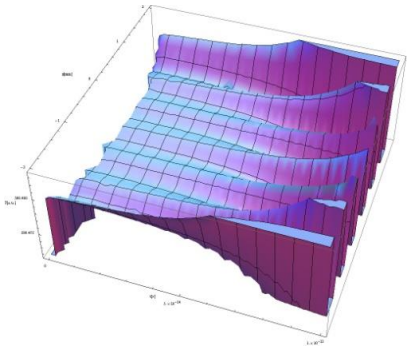

Fig. 10. Thermal field inside the Au bulk target for a single pulse irradiation with a duration of 10^{-13}s, and a relaxation time of 10^{-14}s, for the flat "case" of the laser beam

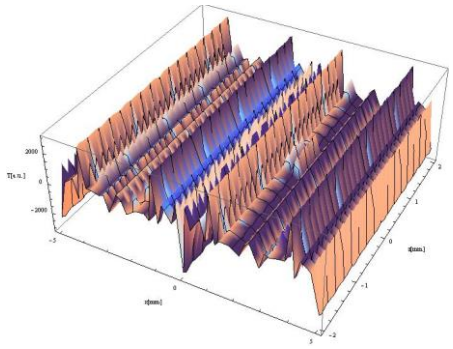

Fig. 11. Temperature field (x - the direction of laser beam propagation, y=0 mm) inside the Au bulk target for a single pulse irradiation of 10^{-13}s, and a relaxation time of 10^{-14s}, for the flat "case" of the laser beam, when $h\rightarrow 0$

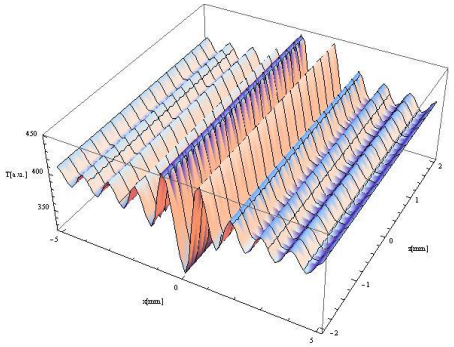

Fig. 12. Temperature field (x - the direction of laser beam propagation, y=0 mm) inside the Au bulk target for a single pulse irradiation of 10^{-13}s, and a relaxation time of 10^{-14}s, for the flat "case" of the laser beam, when h=10-6 $Wmm^{-2}K^{-1}$

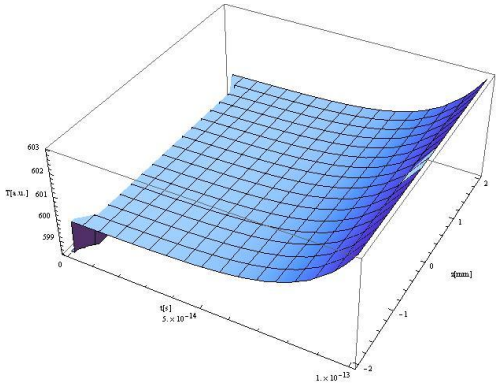

Fig. 13. Thermal field inside the Au bulk target for a single pulse irradiation of 10^{-13}s, and a relaxation time of 10^{-14}s, for the TEM_{00} "case" of the laser beam, when $h\rightarrow 0$

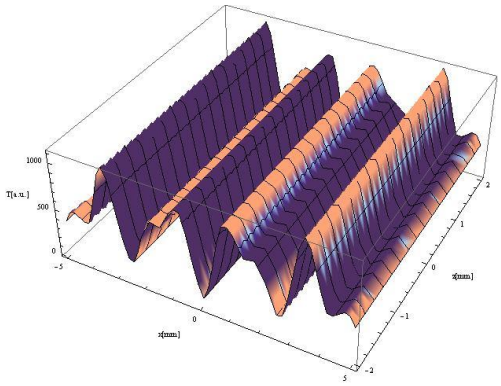

Fig. 14. Temperature field (x - the direction of laser beam propagation, y=0 mm) inside the Au bulk target for a single pulse irradiation of 10^{-13}s, and a relaxation time of 10^{-14}s, for the TEM00 "case" of the laser beam, when h=10-6 $Wmm^{-2}K^{-1}$

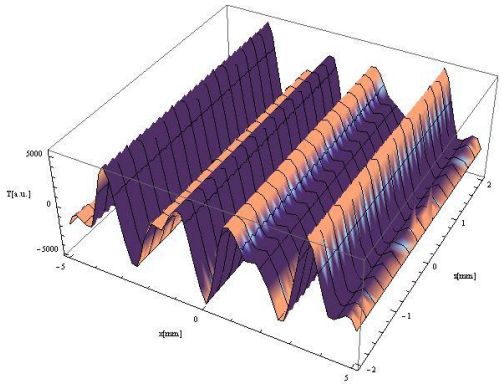

Fig. 15. Temperature field (x - the direction of laser beam propagation, y=0 mm) inside the Au bulk target for a single pulse irradiation of 10^{-13}s, and a relaxation time of 10^{-14}s, for the TEM00 "case" of the laser beam, when h→0

In the last years, especially as far as laser cladding processes are concerned [31], part of the studies has been focusing on the heat transfer when the incident laser beam is in "very exotic" transversal modes intensity.

Finally, Fig. 16 is showing the temperature field (x - the direction of laser beam propagation, y=0 mm) inside the Au bulk target for a single pulse irradiation of 10^{-13}s, and a relaxation time of 10^{-14}s, for the TEM_{30} "case" of the laser beam, when h=10^{-6} $Wmm^{-2}K^{-1}$. Fig. 17 is showing the thermal field inside the Au bulk target for a single pulse irradiation of 10^{-13}s, and a relaxation time of 10^{-14}s, for the TEM_{30} "case" of the laser beam, when h→0.

It can be easily noticed that in normal heat transfer conditions, the spatial anisotropy of TEM_{30} laser mode is producing a spatial anisotropy of the thermal field (Fig. 16). Conversely, in Fig. 17, the thermal field is almost uniform, due to a regime where h→0.

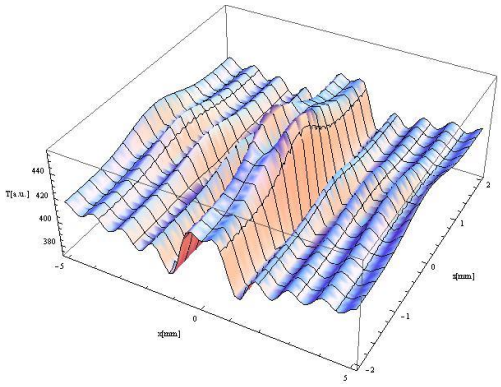

Fig. 16. Temperature field (x - the direction of laser beam propagation, y=0 mm) inside the Au bulk target for a single pulse irradiation of 10^{-13}s, and a relaxation time of10^{-14}s, for the TEM30 "case" of the laser beam, when h=10-6 $Wmm^{-2}K^{-1}$

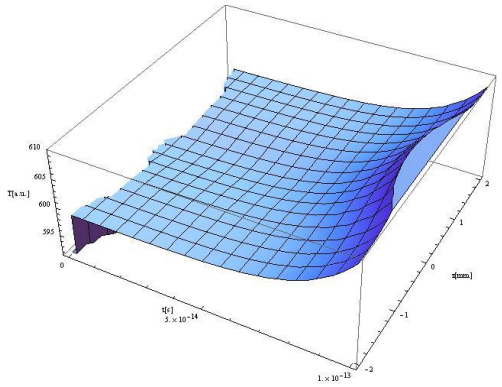

Fig. 17. Thermal field inside the Au bulk target for a single pulse irradiation of 10^{-13}s, and a relaxation time of 10^{-14}s, for the TEM30 "case" of the laser beam, when h→0

6. Conclusions

The new emerging LAM technique aims at producing complex shaped functional components, from metals (mainly Au, Cu, Ag or Al), alloys and metal matrix composite powder materials that cannot be easily fabricated by conventional methods. The purpose is to meet the current demanding requirements from aerospace, automotive, rapid tooling and biomedical industries. LAM technology basically resorts to either Laser sintering, Laser melting or Laser metal deposition [18]. Each LAM process has specific characteristics in terms of materials, procedures, and specific applications [19].

To this purpose, the current team has developed a simple new solution approach for the two-temperature model, which can be used to evaluate the thermal field in laser-matter interaction. In the model proposed, the heat velocity is assumed to be finite. The solutions are analytical, and only the first 10 values of the current indices i, l, j have been taken into account. This involves an absolute error of only 10^{-2} ºC [30]. It is important to mention that the simulations carried out have been performed for rather low heat transfer coefficients, *i.e.* under high vacuum conditions surrounding the target sample [30].

The main results of the analysis performed by the current team are:

1. the maximum value of the temperature field can be varied by changing the relaxation time/ pulse duration;

2. the shorter the relaxation time/pulse duration are, the narrower the temperature field is for the Gaussian and flat "cases";

3. a key role is played by the "balance" between the heat transfer coefficients and the laser transversal intensity modes. If a uniform thermal field is the target, the extreme vacuum condition ($h \to 0$) should be chosen.

These results can be important for a fast design of the laser systems used for LAM, *i.e.* the choice between shorter or longer laser pulses. These requirements are related to the characteristics of the materials/powders to be processed [32]. More specifically, the question that needs answering is whether to apply higher or lower temperature values and more or less uniform temperature distributions. This option will be finally reflected in the quality of the laser-treated zone. Practically, the choice to be made should be between ns, ps and fs pulses in order to perform an optimum LAM process. In any case, a lower residual pressure (higher vacuum) is preferred in order to obtain a uniform temperature field with beneficial effects for LAM.

Acknowledgments

M.O., I.N.M., C.R. and G.P.-P., acknowledge the support of MCI-DGOIC under Contract POC G 135/23.09.2016 (PRELAM).

References

[1] D. D. Joseph, Luigi Preziosi, Rev. Mod. Phys.**61**, 41 (1989).
[2] S. Nolte, C. Momma, H. Jacobs, A. Tunnermann, B. N. Chichkov, B. Wellegehaussen, H. Welling, Journal Optical Society of America B **14**(10), 2716 (1997).
[3] M. Oane, M. Taca, S. L. Tsao, Lasers in Engineering **24**(1-2), 105 (2012).
[4] J. P. Colombier, P. Combis, F. Bonneau, R. Le Harzic, E. Audouard, Physical Review B **71**, 165406 (2005);
[5] I Jong Kim, Ki Hong Pae, Chul Min Kim, Hyung Taek Kim, Jae Hee Sung, Seong Ku Lee, Tae Jun Yu, Il Woo Choi, Chang-Lyoul Lee, Kee Hwan Nam, Peter V. Nickles, Tae Moon Jeong, Jongmin Lee, Transition of Proton Energy Scaling Using an Ultrathin Target Irradiated by Linearly Polarized Femtosecond Laser Pulses, 165003 (2013) Physical Review Letters;
[6] Yuichiro Yamashita, Takehiko Yokomine, Shinji Ebara, Akihiko Shimizu, Fusion Engineering and Design **81,** 1695 (2006).

[7] G. L. Eesley, Physical Review B, **33**(4), 2144 (1986).
[8] T. Balasubramni, S.H. Kim, S.H. Jeong, Applied Surface Science **255,** 9601 (2009).
[9] Mikhail E. Povarnitsyn, Tatiana E. Itina, Konstantin V. Khishchenko, Pavel R. Levashov, Applied Surface Science **253,** 6343 (2007).
[10] Zhibin Lin, Leonid V. Zhigilei, Applied Surface Science **253,** 6295 (2007).
[11] M. Lino da Silva, V. Guerra, J. Loureiro, Chemical Physics **342**, 275 (2007).
[12] N. A. Inogamov, V. V. Zhakhovskii, S. I. Ashitkov, V. A. Khokhlov, Yu. V. Petrov, M. B. Agranat, S. I. Anisimov, K. Nishihara, Applied Surface Science **255,** 9712 (2009).
[13] S. Valette, R. Le Harzic, N. Huot, E. Audouard, R. Fortunier, Applied Surface Science **247,** 238 (2005).
[14] V. Linss, H. Kupfer, S. Peter, F. Richter, Surface & Coatings Technology **200,** 1696 (2005).
[15] R. W. Schoenlein, W. Z. Lin, J. G. Fujimoto, G.L. Eesley, Physical Review Letters **58**(16), 1680 (1987).
[16] B. H. Christensen, K. Vestentoft, P. Balling, Applied Surface Science **253,** 6347 (2007).
[17] V. Damian, M. Oane, A. Bucă, Lasers in Engineering, No. 1-3, 181 (2016).
[18] D. D. Gu, W. Meiners, K. Wissenbach, R. Poprawe, International Materials Reviews **57**(3), 133 (2012).
[19] Dongdong Gu, Springer-Verlag Berlin Heidelberg, 311 pp, 2015.
[20] Andres Gasser, Gerhard Backes, Ingomar Kelbassa, Andreas Weisheit, Konrad Wissenbac, Laser Additive Manufacturing: Laser Metal Deposition (LMD) and Selective Laser Melting (SLM) in Turbo-Engine Applications, **7**(2), WILEY-VCH Verlag GmbH & Co. KGaA, Weinheim, 58 (2010).
[21] M. Oane, D. Sporea, Infrared Physics & Technology **42,** 31 (2001).
[22] M. Oane, A. Peled, F. Scarlat, I. N. Mihailescu, A. Scarisoreanu, G. Georgescu, Infrared Physics & Technology **51,** 242 (2008).
[23] M. Oane, A. Peled, F. Scarlat, I. N. Mihailescu, G. Georgescu, Infrared Physics & Technology **51**, 348 (2008).
[24] M. Oane, F. Scarlat, I. N. Mihailescu, Infrared Physics & Technology, **51,** 344 (2008).
[25] N. S. Koshlyakov, M. N. Smirnov, E. B. Gliner, Differential Equation of Mathematical Physics. Amsterdam: North-Holland Publishing. 1964.
[26] T. Visan, D. Sporea, G. Dumitru, Computing method for evaluating the absorption coefficient of infrared optical elements, vInfrared Physics & Technology **39,** 335 (1998).
[27] M. Oane, D. Ticos, C.M. Ticoş, Scholars' Press - Germany, 2015, "Charged particle beam Processing versus laser processing" ISBN 978-3-639-66753-0, pp.:11, monograph;
[28] M. Oane, A. Peled, R. V. Medianu, Lambert Academic Publishing – Germany, "Notes on Laser Processing" 2013, ISBN 978-3-659-487-48739-2, monograph;
[29] M. Oane, R. V. Medianu and A. Bucă, "Radiation Effects in Materials", pp.: 413-430, 2016, InTech, ISBN: 978-953-51-2417-7, Cap.16"A Parallel between Laser Irradiation and Relativistic Electrons Irradiation of Solids", monograph;
[30] M. Oane, K. Vutova, I. N. Mihailescu, V. Donchev, G. Florescu, L. Munteanu, G. Georgescu, Vacuum **86**, 1440 (2012).
[31] W.C. Tseng, J. N. Aoh, The Open Mechanical Engineering Journal **8**, 370 (2014).
[32] W. M. Steen, J. Mazumder, Laser Material Processing, Springer, 2010, ISBN 978-1-84996-061-8, monograph;